*Investigation of oxidation profile in PMR-15 polyimide using atomic force microscope (AFM)

Lili L. Johnson* and R. K. Eby

Department of Polymer Science, University of Akron, Akron, OH 44325-3909

Mary Ann B. Meador

Materials Division, NASA Glenn Research Center, Cleveland, OH 44135

Nanoindentation measurements are made on thermosetting materials using cantilever deflection vs. piezoelectric scanner position behavior determined by AFM. The spring model is used to determine mechanical properties of materials. The generalized Sneddon's equation is utilized to calculate Young's moduli for thermosetting materials at ambient conditions. Our investigations show that the force-penetration depth curves during unloading in these materials can be described accurately by a power law relationship. The results show that the accuracy of the measurements can be controlled within 7%. The above method is used to study oxidation profiles in PMR-15 polyimide. The thermo-mechanical profiles of PMR-15 indicate that the elastic modulus at the surface portion of the specimen is different from that at the interior of the material. It is also shown that there are two zones within the oxidized portion of the samples. Results confirm that the surface layer and the core material have substantially different properties.

* lljohn@aestpe.com;(330)849-5195(Telephone);(330)849-5597(Fax)

(Keywords: nanomechanical properties; PMR-15 polyimide; atomic force microscopy)

INTRODUCTION

Atomic force microscope (AFM),[1] also known as the scanning force microscope (SFM), is one of the most successful scanning probe microscopes (SPMs), which encompasses a family of instruments used to study surface topography and surface properties of materials on a very fine scale.[2-4] It has been an indispensable analytical tool for obtaining high-resolution images of conductive and non-conductive surfaces. The development of the AFM imaging capabilities has focused on the effects of the tip-surface interaction forces on images, leading to the utilization of the AFM as a surface force apparatus. The forces include repulsive, van der Waals, magnetic, electrostatic and capillary forces.[5-9] The ability to measure the interaction as a function of separation distance between the tip and the sample surface leads to the configuration of an AFM into a nanoindenter.[10] This allows the AFM to characterize the deformation characteristics of the materials via nanoindentation at shallow depths and low loads. The methodology of obtaining mechanical properties such as elastic modulus of materials in the literature has focused on indentation with conventional indenters in materials science and engineering.[11, 12] Since AFM is a relatively new instrument, the instrumental ability to probe mechanical properties of materials needs to be evaluated and documented.

Polyimides based on the PMR (polymerization of monomeric reactants) approach are used as high temperature resistant polymer matrix materials for aircraft engine applications,[13] since they combine ease of processing, high specific strength and modulus with good oxidative stability up to 316 °C. The thermo-oxidative stability (TOS) of

PMR-15 polyimide has been assessed using classical methods and modern instruments.[14-22] Physical changes of PMR-15 polyimide upon aging have been examined by weight loss measurement, light optical microscopy (LM), and scanning electron microscopy (SEM). X-ray photoelectron spectroscopy (XPS), Fourier transform infrared (FTIR) spectroscopy, and nuclear magnetic resonance (NMR) spectroscopy have been used to study chemical changes of PMR-15 polyimide upon aging. There is little assessment on microscopic spatial variations of PMR-15 polyimide due to oxidation in the literature. Our purpose in this research is to carry out studies in the areas: (1) develop and improve the methodology of using AFM as a nanoindentation technique; (2) utilize elastic theories to calculate the Young's modulus of polymeric materials; (3) investigate the oxidation profile in PMR-15 polyimide.

EXPERIMENTAL

Sample preparation

PMR-15 polyimide plates (100 × 100 × 1.5 mm) were compression molded from an imidized powder commercially available from HyComp of Cleveland, Ohio. A charge of 30 g of material was loaded into a steel tool that was then placed between the plates of a hydraulic press preheated to 232 °C. Stops were used to prevent pressure on the material until the mold temperature reached 232 °C. At this point, the stops were withdrawn and contact pressure was applied and held for 10 min. After this hold, a pressure of 240 psi was applied and the temperature ramped up to 315 °C. When the die temperature reached 300 °C, the pressure was increased to 500 psi. The part was held under these conditions for 2 h, after which it was allowed to cool to below 232 °C before removal. The resulting

PMR-15 polyimide plate was cut into specimens (nominally 10 × 10 × 1.5 mm) using a diamond wheel. All edge material was discarded to avoid any anomalous effects.

Nine samples were selected for isothermal aging. Three air-circulating ovens were set at the temperatures of 315 °C, 330 °C, and 343 °C respectively. Three samples were placed in the middle area of each oven. The airflow rate for the ovens was controlled to be 100 cm^3/min.. The aging periods for the samples were nominally 100 h, 200 h, and 300 h.

Prior to indentation measurements using the AFM, the PMR-15 polyimide samples either unoxidized or oxidized were mounted into epoxy to form cylinders 25 mm in diameter and 19 mm in length. The samples were mounted in a way that the cross-section of the samples is near the surface of the 25-mm diameter. These cylinders were polished to expose the thickness of the PMR-15 polyimide materials and to achieve optical smoothness of the exposed internal sample surface. These samples were then cut by a diamond saw in a very mild lubricant into 4 × 4 × 1.5 mm pieces with the polished interior surface preserved. The small sized samples were then washed by DAWN® brand concentrated dish liquid and thoroughly rinsed by distilled water. The samples were then dried under a hood and put into a desiccator under vacuum condition for later use.

AFM as a nanoindentation technique

The TopoMetrix 2100 AFM used in this work is a commercial AFM made by TopoMetrix Inc. of Santa Clara, CA. (Now part of Thermomicroscopes of Santa Clara). A schematic diagram of the main components of an AFM is shown in *Figure 1*. In this technique, the laser beam from a laser diode reflects from the mirror onto the back of the

cantilever, then the beam reflects from the back of the cantilever onto the position-sensitive photodiode detector. As the cantilever bends due to the forces between the tip and the sample, the position of the laser beam on the detector shifts. The changing detected signal is recorded in nanoampere (nA).

In this study, the sample is located on top of a tripod piezoelectric scanner that provides sample positioning in z direction. The sample movement in the x-y plane is accomplished with a translator beneath the tripod scanner.

Force measurements are made in contact AFM by monitoring the deflection of a flexible element (usually a cantilever) in response to the interaction forces between the tip (normally integrated with the free end of the cantilever) and the sample. Because of the sensitivity of the photodiode detector involved, the cantilever should have a spring constant (typically $10^{-2} - 10^{3}$ N/m) that is measurable. In this study, I-shaped single crystal silicon probes with the tip geometry of an asymmetrical four-side pyramidal shape (Nanosensors GmbH, in Germany) were used. The spring constant of these probes is in the range of 0.30 – 600 N/m. These probes also have a high resonant frequency (20 – 500 kHz). The mechanical quality factor (Q) of these probes is in the range of 100 – 1000.

In the indentation experiment of AFM, the probe-sample interaction is simulated as two springs in series, the spring model approach,[23] as shown in *Figure 2*. After contact is made between the probe tip and the sample surface, the relationship between the total displacement of the piezoelectric scanner (ΔZ_p), the displacement due to tip deflection (ΔZ_t), and the indentation displacement due to sample deformation (ΔZ_i) is simply

$$\Delta Z_p = \Delta Z_t \times \cos(\alpha) + \Delta Z_i \quad (1)$$

where α is the angle between the cantilever and the horizontal axes and the tip deflection can be directly related to the applied force, F, by

$$F = \Delta Z_t \times \cos(\alpha) \times k_c \quad (2)$$

where k_c is the spring constant of the cantilever. Since the optical detection system is used to record the cantilever displacement, the unit of cantilever displacement has to be converted from nA into nm to study mechanical properties of materials.

To convert the unit of cantilever deflection, a sample, such as sapphire, which is effectively infinitely stiff with respect to the cantilever probe is used. In this case, the assumption made is that there is no indentation in the sample and the piezo displacement is totally contributed to the tip displacement, i.e. $\Delta Z_p = \Delta Z_t$.

From simple beam theory, the angle change ($\Delta\theta_t$) and the tip displacement (ΔZ_t) are related by

$$\Delta\theta_t = (3\Delta Z_t)/(2L_c \times \cos(\alpha)) \quad (3)$$

where L_c is the length of the cantilever probe. This angle change is directly related to the change in tip deflection current (A_{td}) by system conversion and amplification factors, which can be lumped into a constant, C_θ, such that

$$\Delta\theta_t = (\Delta A_{td})/C_\theta \quad (4)$$

combining equations (3) and (4), the slope of the deflection curve, S, is shown to have an upper limit, S*, given by

$$S^* = (\Delta A_{td})/(\Delta Z_p) = (3C_\theta)/(2L_c \times \cos(\alpha)) \quad (5)$$

The Young's modulus of a material is calculated using Sneddon's equation[24] from continuous indentation experiment if the indentation behavior of the material is elastic. For materials that exhibit not only elastic behavior but also plastic under indentation experiments, Sneddon's approach does not apply. Instead, a generalized form of Sneddon's equation[11] better describes the unloading behavior of these materials.

$$F = [(\xi \times E)/(1-\upsilon^2)] \times (h-h_f)^n \quad (6)$$

where F is the applied load (nN), ξ is dependent on the contact geometry, E is the Young's modulus (Pa), υ is the Poisson's ratio, h is the current penetration depth (nm), h_f is the final depth of the contact impression after unloading (nm), and n is the tip geometry. This generalized Sneddon's equation is used to study the unloading behavior of thermosets in this work.

RESULTS AND DISCUSSION

Evaluation of AFM as a nanoindentation technique

The cantilever deflection-piezoelectric scanner displacement behavior of a sapphire sample was investigated first using an I-shaped silicon probe (46#6) to test the reliability of the atomic force microscope in this experiment. In *Figure 3*, cantilever deflection (nA) is plotted as a function of piezoelectric scanner position (nm) for a sapphire sample. It is seen that the cantilever deflection remains unchanged before the tip-sample contact is made. After the tip contacts the sample, the cantilever deflection increases with the extension of the piezoelectric scanner in the loading process. It decreases with the retraction of the piezoelectric scanner in the unloading process and returns to its equilibrium position after the tip breaks free of the sample. It is also seen that the unloading path retraces the loading path. It indicates the linear behavior of the piezoelectric scanner and the position sensitive photodiode detector.

In *Figure 4*, the cantilever deflection (nA) is plotted as a function of piezoelectric scanner position (nm) for the deflected portion of the loading curve in *Figure 3*. Linear regression is used to fit the deflection data. The slope (nA/nm) is defined as the cantilever sensitivity and used to convert the deflection unit from nA to nm. Because sapphire can be considered as an infinitely hard sample compared to the stiffness of the cantilever of the silicon probe, the cantilever deflection of the probe increases or decreases linearly with the extending or retracting of the piezoelectric scanner position. There is no penetration of the tip into the sapphire sample. Therefore, the linear coefficient of the data is taken as the cantilever sensitivity. Ten sets of data were

collected at different locations on the sapphire sample. The average value of the cantilever sensitivity is utilized throughout this study.

The cantilever deflection as a function of piezoelectric scanner position behavior of a commercially available epoxy was investigated. This material is chosen to be a reference sample for evaluating AFM as a nanoindentation technique for thermosetting materials. There are three reasons for choosing this material as a reference sample. First, epoxy is a widely used thermosetting material and its mechanical properties can be obtained readily from the literature. Second, with the known modulus and Poisson's ratio of epoxy, the contact geometry and tip geometry parameters of epoxy can be calculated from the generalized Sneddon's equation. Third, since PMR-15 polyimide is also a thermosetting material, the contact geometry parameters calculated for epoxy can be assumed to be the same for PMR-15 polyimide if the experimental conditions are set the same. The Poisson's ratio of these two materials can also be considered to be the same. Therefore, the elastic modulus of PMR-15 polyimide can be calculated from the generalized Sneddon's equation. The cantilever deflection as a function of piezoelectric scanner position for an epoxy sample indented by a silicon probe is presented in *Figure 5*. It is observed that the silicon probe remains at its equilibrium condition before the tip makes contact with the sample. Starting at the contact point, the cantilever deflection increases with the extension of the piezoelectric scanner till a predetermined maximum load is reached, then the cantilever deflection decreases with retraction of the piezoelectric scanner and returns to its equilibrium condition after the tip detaches from the sample. After tip-sample contact is made, the piezoelectric scanner position (nm) includes not only the penetration depth of the epoxy sample but also the cantilever deflection of the

silicon probe. The penetration depth of the epoxy sample is calculated using the spring model and the unit of the cantilever deflection is converted using the cantilever sensitivity parameter.

The cantilever deflection (nm) as a function of penetration depth (nm) behavior of epoxy is plotted in *Figure 6*. It shows that the cantilever deflection increases with increasing penetration depth in the loading process and decreases with decreasing penetration depth in the unloading process. When the load returns to zero, there is a final depth in the unloading curve. This final penetration depth is due to plastic deformation of epoxy. The plastic deformation is included in the generalized Sneddon's equation for materials in indentation experiments. Therefore, the unloading data of the epoxy sample is fitted with the generalized Sneddon's equation.

The force (nN) as a function of displacement (nm) behavior of epoxy is indicated in *Figure 7*. The power law coefficient is used to calculate the contact geometry parameter (ξ) with the known values of elastic modulus and Poisson's ratio of epoxy. The power law exponent provides the tip geometry parameter (n). Ten sets of loading-unloading curves were performed at ten different locations on the epoxy sample. The average values of the geometry parameters of epoxy sample are used.

The cantilever deflection (nA) versus piezoelectric scanner position (nm) behavior of PMR-15 polyimide is investigated not only for the reason of testing the reliability of the instrument but also for extracting the elastic modulus using the generalized Sneddon's equation.

Figure 8 shows the cantilever deflection (nA) as a function of piezoelectric scanner position (nm) of un-oxidized PMR-15 polyimide. It is seen that the loading and

unloading behavior of un-oxidized PMR-15 polyimide is similar to that of the epoxy sample. The cantilever deflection (nm) – penetration depth (nm) behavior of un-oxidized PMR-15 in *Figure 9* shows similar trends compared with that of epoxy sample. A finite penetration depth is also observed in the unloading process. This final penetration depth is due to the plastic deformation of un-oxidized PMR-15 polyimide in the loading process.

To calculate the elastic modulus of un-oxidized PMR-15 polyimide, the force (nN) as a function of the nth power of the displacement ((nm)^n) is plotted using the unloading data of un-oxidized PMR-15 polyimide in *Figure 10*. It is seen that the force has a linear relationship with the nth power of the displacement. The linear coefficient contains the elastic modulus value of un-oxidized PMR-15 polyimide. By assuming the same contact geometry parameter and Poisson's ratio as that for epoxy sample, the elastic modulus of un-oxidized PMR-15 polyimide is calculated. Ten sets of loading-unloading curves of PMR-15 polyimide were performed at ten different locations and data were processed using spring model and the generalized Sneddon's equation. The average elastic modulus (3.31 ± 0.11 GPa) is compared with that (3.24 GPa)[25] of PMR-15 polyimide from the literature and the deviation is about 7%.

To evaluate the repeatability of the indentation technique of AFM, another silicon probe (56#2) of the same type as 46#6 is selected. Indentation measurements were made on sapphire, epoxy, and PMR-15 polyimide under the same experimental conditions. Data were collected at three different times. The average values of the contact geometry parameters (ξ and n) from epoxy and the elastic modulus (E) from PMR-15 polyimide are listed in *Table 1*. It is seen that consistent results are obtained at the three different dates.

The tips of these probes used in this study are in the form of a four-sided pyramid. It is necessary to evaluate the consistency of the tip geometry of these probes since irregular tip geometry will cause erroneous measurements in indentation by AFM.[26] In order to evaluate the consistency of the geometry, four silicon probes (46#6, 56#2, 32#1, and 32#3) were used and the samples were sapphire, epoxy, and un-oxidized PMR-15 polyimide. The average values of the geometry parameters obtained from epoxy samples and elastic moduli obtained from un-oxidized PMR-15 samples are listed in *Table 2*. It shows that while geometry parameters vary somewhat from probe to probe, the determined values of the modulus for the PMR-15 samples are more consistent.

It has been reported that the calculated elastic modulus of materials may change with changing penetration depth due to tip defects.[12, 26] Therefore, in this work, the elastic modulus of PMR-15 polyimide as a function of penetration depth is plotted in *Figure 11*. It is seen that the elastic modulus of un-oxidized PMR-15 polyimide does not change with changing penetration depth if the geometry terms corresponding to the depth are used.

Investigation of oxidation profile in PMR-15 polyimide

Weight loss measurement has been a classical method to estimate the oxidation behavior of PMR-15 polyimide. Weight loss (%) of the PMR-15 polyimide specimens aged at 315, 330, and 343 °C as a function of aging time (h) is shown in *Figure 12*. It is seen that the weight loss increases with increasing aging temperature. The initial weight loss is faster than that near the end of the test for the samples aged at three temperatures. In *Figure 13*, data are displayed on a weight-loss-rate basis. At all three temperatures, the

curves are characterized by a relatively rapid initial weight loss rate that decreases as the aging time progresses and then becomes nearly constant. Similar results for PMR-15 polyimide samples aged at different temperatures and time scales have been reported.[14, 17] The weight loss phenomena of PMR-15 polyimide have been related to the chemical changes during oxidative attack.[21]

Figure 14 shows a cross-section of a specimen that is not aged. It is seen that this sample exhibits uniformity from the sample surface to the interior of the sample, indicating there is no oxidation effect in this sample. The cross-sections shown in *Figures 15 to 23* of aged samples show presence of a distinct layer that develops and grows on the polymer specimen surface due to oxidation at different aging times at elevated temperatures. It is observed that this layer thickens with aging time and temperature. Also, voids are observed in this layer. The size and the amount of voids increase with increasing aging time and temperature. Similar observations have been documented in the literature.[14]

It has been discussed that the polymer oxidation process appears to entail the concurrent formation of a surface layer that is structurally different from the interior of the specimen, which is the same as the initial cured polymer material. There is also a formation and growth of voids in this surface layer. The formation of the voids is related to the gaseous byproducts released during oxidation of the polymer.[17, 21]

Modulus (GPa) as a function of position from sample surface (μm) for PMR-15 polyimide samples aged in air at 315 °C at three different time scales is plotted in *Figure 24*. The modulus profile of un-oxidized PMR-15 polyimide is also included for comparison. It is seen that the elastic modulus of the latter is about constant as the probe

moves from the sample surface towards the interior of the sample. However, each of the aged samples show up to three distinct zones on the oxidation profiles along the sample thickness.

In the region closest to the surface, the data for each sample is constant in to a certain depth. The layer represented by this "plateau" can be referred to as the homogeneously oxidized layer, which is the result of a zero order reaction. Beneath this reaction zone, the modulus decreases as the probing position moves towards the interior of the sample and at some point merges with that of un-oxidized PMR-15 polyimide. This reaction zone could be considered as the diffusion-controlled oxidation zone, which is the result of a first order reaction. After the merge, the modulus of the inner material has been found to be unchanged by oxidation reaction. This is in agreement with microscopic FTIR data [17] which shows that polymer in the outer layer has undergone complete oxidation but the interior is unchanged chemically from unaged samples.

Modulus profiles of PMR-15 polyimide samples aged in air at 330 °C for three different time scales are presented in *Figure 25*. It indicates that the homogeneously oxidized layer is present for samples aged at 100 h and 200 h, but not for the sample aged for 300 h. (The absence is more obvious in the data for aging at 343 °C given in *Figure* 26.). In addition, the thickness of the homogeneously oxidized layer increases with increasing aging time from 100 h to 200 h. The absence of the homogeneously oxidized layer for the sample aged for 300 h could be due to presence of voids developed at the sample surface at longer aging time and higher temperature.

In *Figure 26*, the modulus profiles are presented for sample aged in air at 343 °C for 100 h, 200 h, and 324 h. It shows that the homogeneously oxidized layer is not observed for these three samples.

Figures 27 and 28 show the temperature effect of the modulus profiles of PMR-15 polyimide samples aged for 100 h and 200 h respectively. It is seen that the thickness of the homogeneously oxidized layer decreases with increasing aging temperature.

The modulus profiles observed in this study are similar to profiles seen by Dole and Chauchard using pinpoint DMA of heterogeneously aged poly(ethylene-co-methylacrylate)-based elastomer.[17] Dole and Chauchard discussed a general solution for the theoretical oxidation profile based on rate of oxidation reaction and rate of diffusion of oxygen. In their model, the oxygen concentration profile is as shown in *Figure 29*. Critical oxygen concentration, $[O_2]_c$, is defined as the amount necessary to oxidize the polymer at the maximum rate. Four cases can exist. In case I, the oxygen concentration at the surface is lower than $[O_2]_c$ therefore, the oxidation rate is lower than the maximum. Hence, the modulus decreases steadily from the surface to the center of the sample. For case II, the oxygen concentration at the sample surface is equal to $[O_2]_c$. Again, the modulus decreases steadily from the surface to the interior, but it is higher at the surface than in Case I. For Case III, the oxygen concentration at the surface is much higher then $[O_2]_c$. In this case a fraction of the sample forms a homogeneously oxidized layer where oxidation is controlled by rate of reaction rather than diffusion of oxygen. Proceeding further into the sample, is a diffusion controlled layer as seen in Cases I and II where the oxygen concentration is again below $[O_2]_c$. Case IV is the condition in which oxygen

concentration throughout the sample is above $[O_2]_c$, and therefore oxidation is homogeneous throughout the sample.

In this study, samples of PMR-15 aged at 315 °C fit Case III. In each of these samples, a homogeneous oxidation layer is obtained but grows in depth with increasing aging time. At higher temperatures, the profiles fit Case I or II. No homogeneous oxidation layer is produced because the maximum rate of oxidation increases with increasing temperature, hence the $[O_2]_c$ is never reached.

CONCLUSIONS

In this work, the results of carefully designed and executed experimental investigations have been reported. The experimental study consists two parts. The first part is focused on evaluation of AFM as a nanoindentation technique. Particular attention was focused on extracting the elastic modulus of polymeric materials. The second part is focused on investigation of oxidation profile in PMR-15 polyimide using AFM as a nanoindenter. The effects of temperature and time on PMR-15 polyimide oxidation behavior were studied.

Results from the first part indicate that the generalized Sneddon's equation can be used to describe accurately the unloading behavior of thermosetting materials. The power law exponent is about 2 suggesting that the flat punch method of analysis for determining modulus from indentation force-penetration depth data is not entirely adequate. The contact geometry and tip geometry parameters (ξ and n) obtained using four silicon probes show fairly consistent tip shape for this type of probe. The elastic modulus of un-oxidized PMR-15 polyimide obtained using four silicon probes indicates the parameters

to be independent of penetration depth. The moduli computed by this method are within 7% of the values reported by independent means.

In the second part of the investigation, detailed modulus profiles in PMR-15 polyimide samples aged at different temperatures and time scales are established confirming that AFM is capable of mapping mechanical property variations in polymers. The modulus profiles in PMR-15 polyimide samples aged at 315 °C for 100 h, 200 h, and 344 h and 330 °C for 100 h and 200 h show diffusion independent (zero order reaction) and diffusion-controlled (first order reaction) oxidation processes. The modulus profiles of PMR-15 polyimide samples aged at 343 °C indicate the absence of the diffusion independent zone and only the diffusion-controlled process.

ACKNOWLEDGEMENTS

This research was carried out by the financial support of NASA Glenn Research Center, under the HOT-PC program which is gratefully acknowledged.

REFERENCES

1 C. Binnig, C. F. Quate, and Ch. Gerber, *Phys. Rev.Lett.* **12,** 930 (1986).

2 O. Marti and M. Amrein, "STM and SFM in Biology", Academic Press, Inc. London, 1993.

3 R. Wiesendanger, "Scanning Probe Microscopy and Spectroscopy", VCH Press Syndicate of the University of Cambridge, NY, 1994.

4 S. N. Magonov and M-H. Whangbo, "Surface Analysis with STM and AFM", VCH Verlagsgesellschatt mbH, Germany, 1996.

5 L. W. Bruch, *Surf. Sci.* **125,** 194 (1983).

6 H. Bengel, H. –J. Cantow, S. H. Magonov, H. Hillebrecht, G. Thiele, W. Liang, and M. –H. Whangbo, *Surf. Sci.* **343,** 95, (1995).

7 Y. Martin, C. C. Williams and H. K. Wickramasinghe, *J. Appl. Phys.* **61,** 4723 (1987).

8 Y. Martin and H. K. Wickramasinghe, *Appl. Phys. Lett.* **50,** 1455 (1987).

9 J. E. Stern, B. D. Terris, H. J. Mamin and D. Rugar, *Appl. Phys. Lett.* **53,** 2717 (1988).

10 N. A. Burnham and R. J. Colton, *J. Vac. Sci. Technol.* **A7,** 2906 (1989).

11 W. C. Oliver and G. M. Pharr, *J. Mater. Res.*, **7,** 1564 (1992).

12 B. J. Briscoe, K. S. Sebastian and M. J. Adams, *J. Phys. D: Appl. Phys.*, **27,** 1156 (1994).

13 M. A. Meador, P. J. Cavano and D. C. Malarik, *Proceedings of the Sixth Annual ASM/ESD Advanced Composites Conference,* 529, 1990.

14 K. J. Bowles, D. Jayne and T. A. Leonhardt, *SAMPE QUARTERLY,* January, 2, 1993.

15 W. B. Alston, R. E. Gluyas and W. J. Snyder, "Cyclopentadiene Evolution During Pyrolysis-Gas Chromatography of PMR Polyimides." NASA TN 105629, AVSCOM T. R. 91-C-023.

16 G. D. Roberts, D. C. Malarik and J. O. Robaidek, "Viscoelastic Properties of Addition-Cured Polyimides Used in High Temperature Polymer Matrix Composites," composites Design, Manufacturing, and Application; Proceedings of the Eighth International Conference on Composite Materials, S. W. Tsai and G. S. Springer, eds., Soc. for Adv. Mater. and Process Eng., Covina, CA, 12-H-1, 1991.

17 M. A. B. Meador, C. E. Lowell, P. J. Cavano and P. Herrera-Fierro, *High Perform. Polym.* **8,** 363 (1996).

18 J. N. Hay, J. D. Boyle, S. F. Parker, and D. Wilson, *Polymer,* **30,** 1032 (1989).

19 W. B. Alston, R. E. Gluyas and W. J. Snyder, *NASA Technical Memorandum 105629,* 1992.

20 M. Simpson, P. M. Jacobs and F. R. Jones, *Composites,* **22,** 105 (1991).

21 M. A. B. Meador, J. C. Johnston, P. J. Cavano and A. A. Frimer, *Macromolecules,* **30,** 3215 (1997).

22 M. A. Meador, C. E. Lowell, J. C. Johnston, P. J. Cavano, and P. Herrera-Fierro, *HITEMP Review 1995: Advanced High Temperature Engine Materials Technology Program;* J. R. Gray and C. A. Ginty, Eds.; NASA Conference Publication 10178, paper 8, pp 1-12 (1995).

23 M. R. VanLandingham, S. H. McKnight, G. R. Palsese, R. F. Eduljee, J. W. Gillespie and R. L. JR. McCulough, *Journal of Materials Science Letters,* **16,** 117 (1997).

24 I. N. Sneddon, *Int. J. Eng. Sci.* **3,** 47 (1965).

25 S. H. Goodman, in Handbook of Thermoset Plastics, Noyes Publications, NJ 07656, pp310, 1986.

26 Mareanukroh, Ph.D. Dissertation, University of Akron, 1999. M. Mareanukroh, R. K. Eby, R. J. Scaruzzo, D. R. Hamed, and J. Preuschen, Rubber Chem. & Tech., **73**, 801 (2000).

27 P. Dole and J. Chauchard, *Polymer Degradation and Stability*, **47**, 411 (1995).

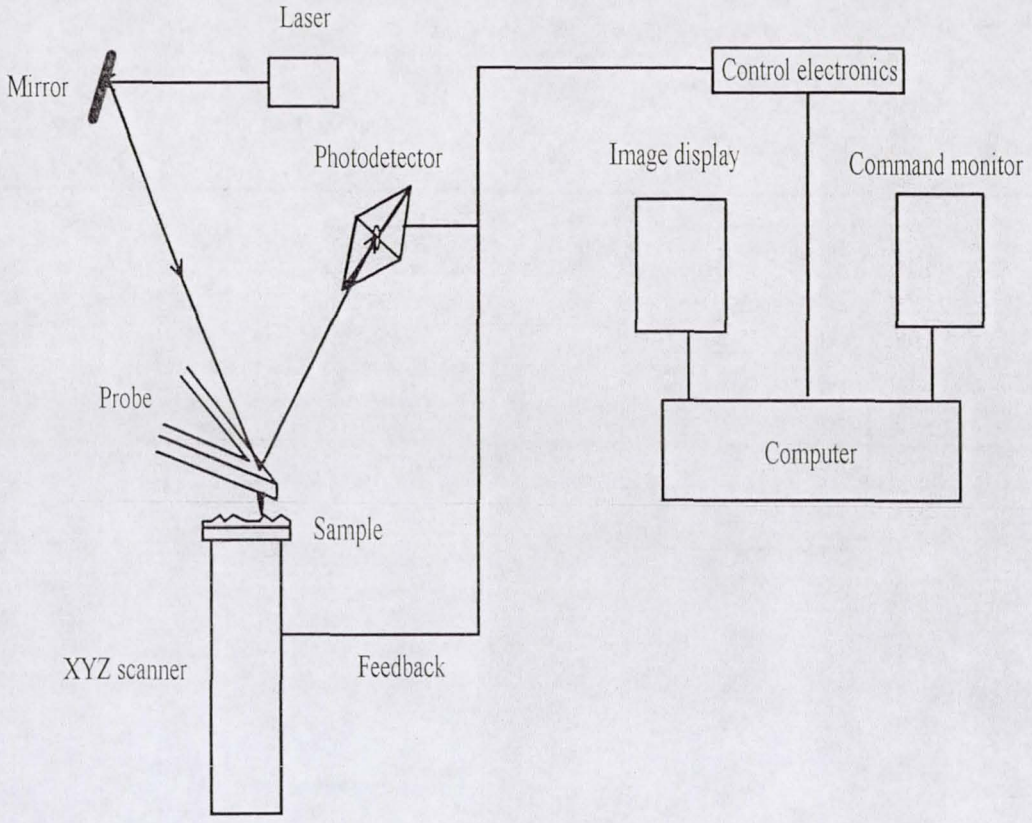

Figure 1 A schematic representation of the main components of an AFM

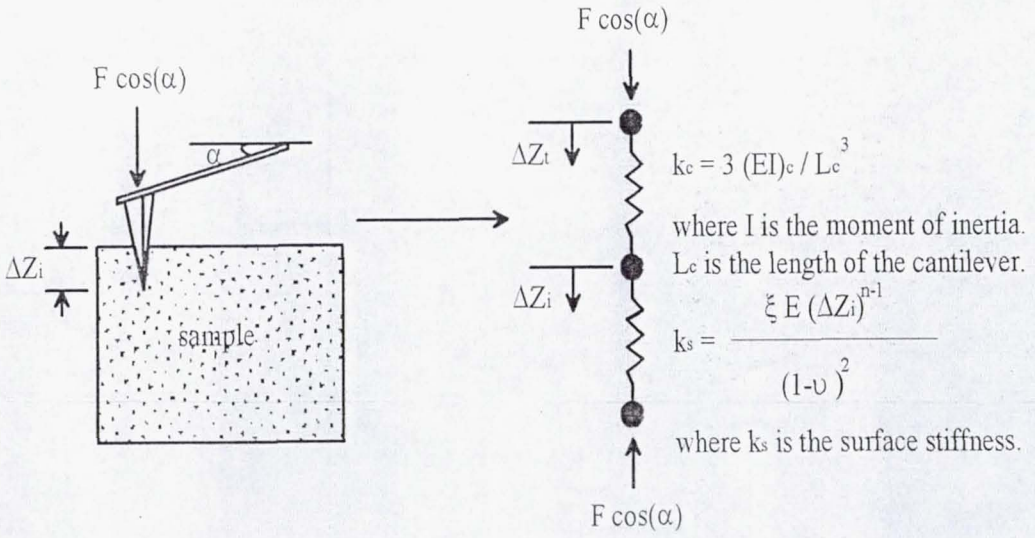

Figure 2 A schematic diagram of the spring model [23]

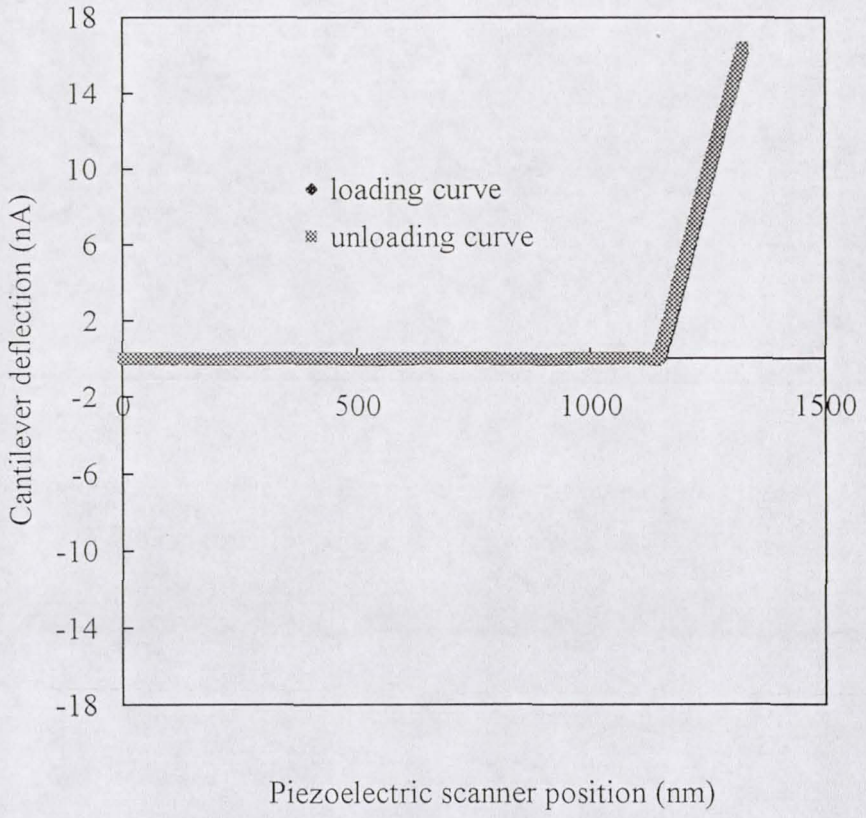

Figure 3 Cantilever deflection (nA) vs. piezoelectric scanner position (nm) of a silicon probe (46#6) on a sapphire sample using the TopoMetrix TMX 2100

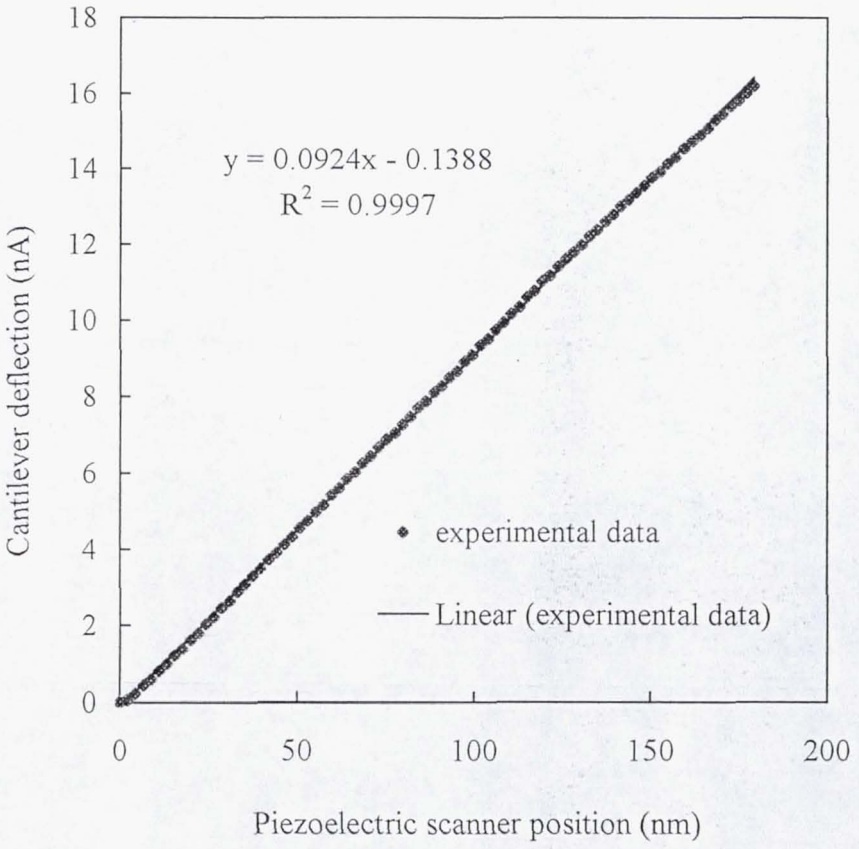

Figure 4 Cantilever deflection (nA) vs. piezoelectric scanner position (nm) for a silicon probe (46#6) on a sapphire sample used to determine the cantilever sensitivity with the TopoMetrix TMX 2100

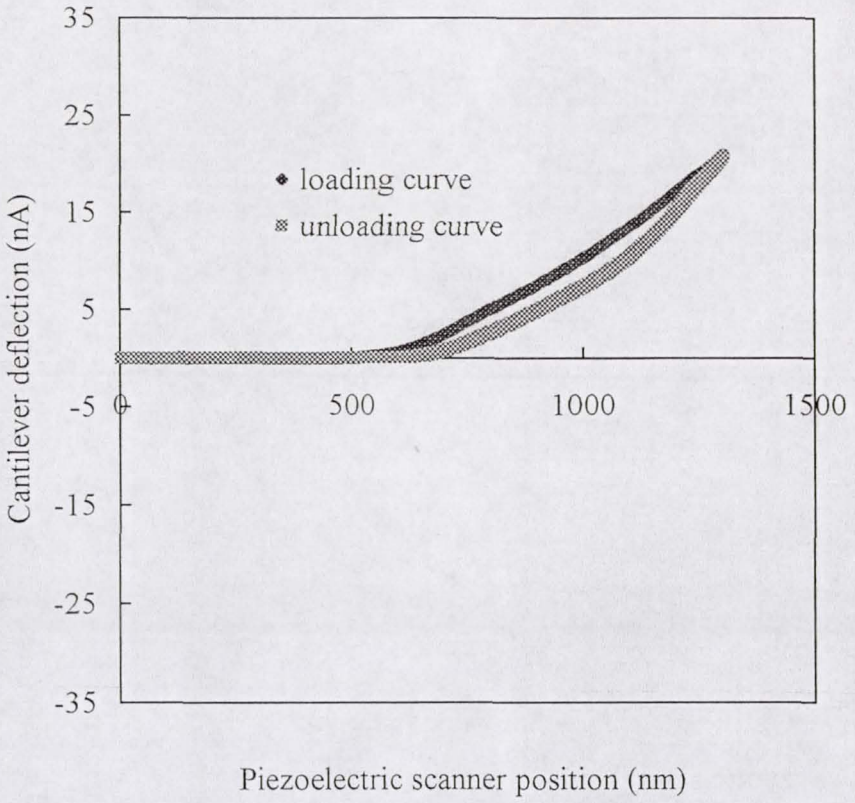

Figure 5 Cantilever deflection (nA) vs. piezoelectric scanner position (nm) of an epoxy sample using a silicon probe (46#6) with the TopoMetrix TMX 2100

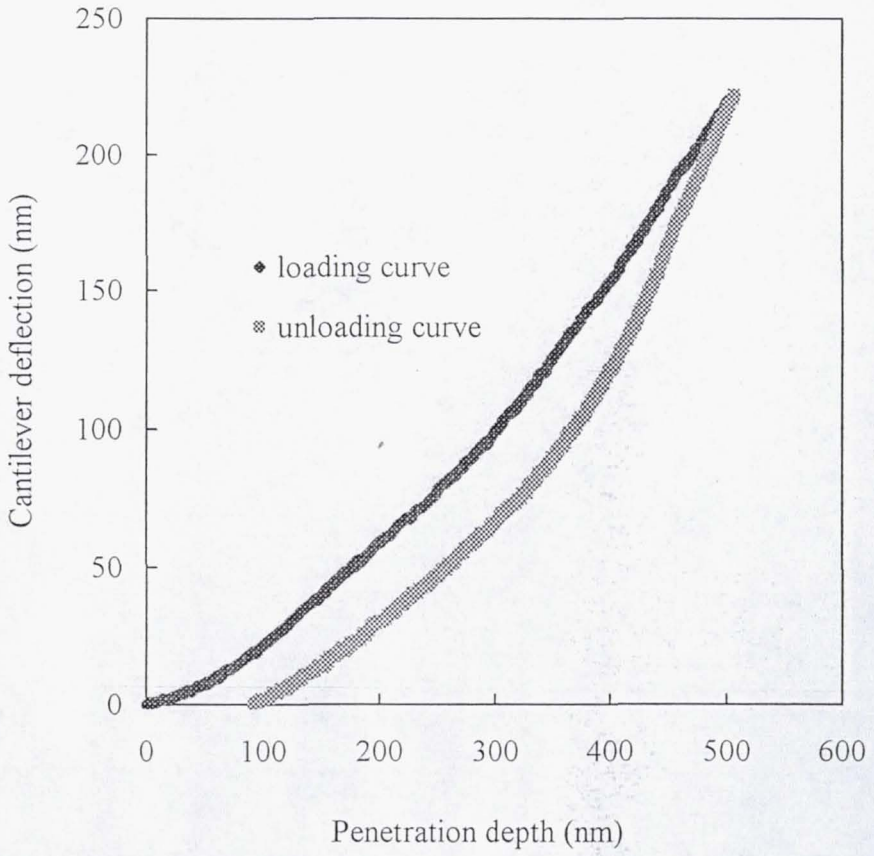

Figure 6 Cantilever deflection (nm) vs. penetration depth (nm) of an epoxy sample using a silicon probe (46#6) with the TopoMetrix TMX 2100

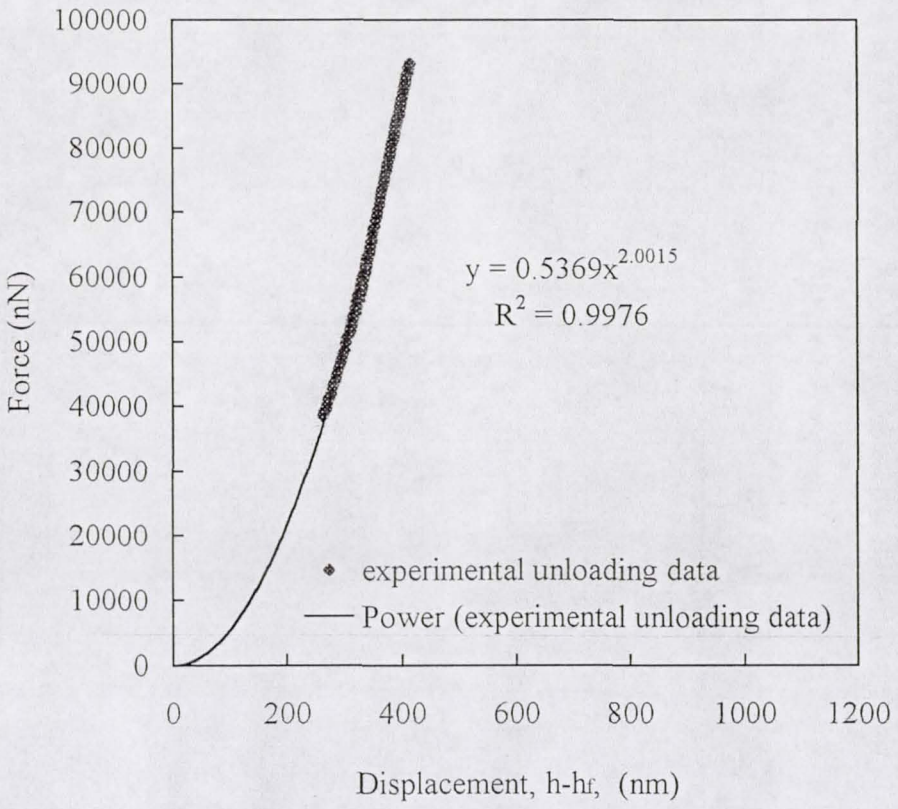

Figure 7 Force (nN) vs. displacement between the current penetration depth and the final depth (nm) of an epoxy sample using a silicon probe (46#6) with the TopoMetrix TMX 2100

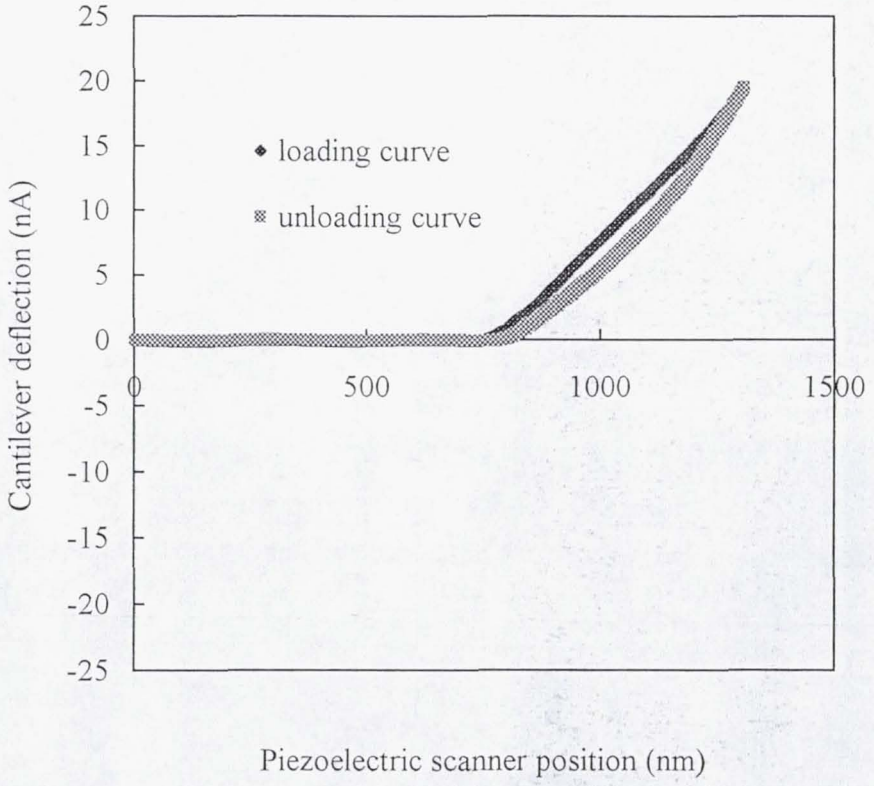

Figure 8 Cantilever deflection (nA) vs. piezoelectric scanner position (nm) of an un-oxidized PMR-15 polyimide sample using a silicon probe (46#6) with the TopoMetrix TMX 2100

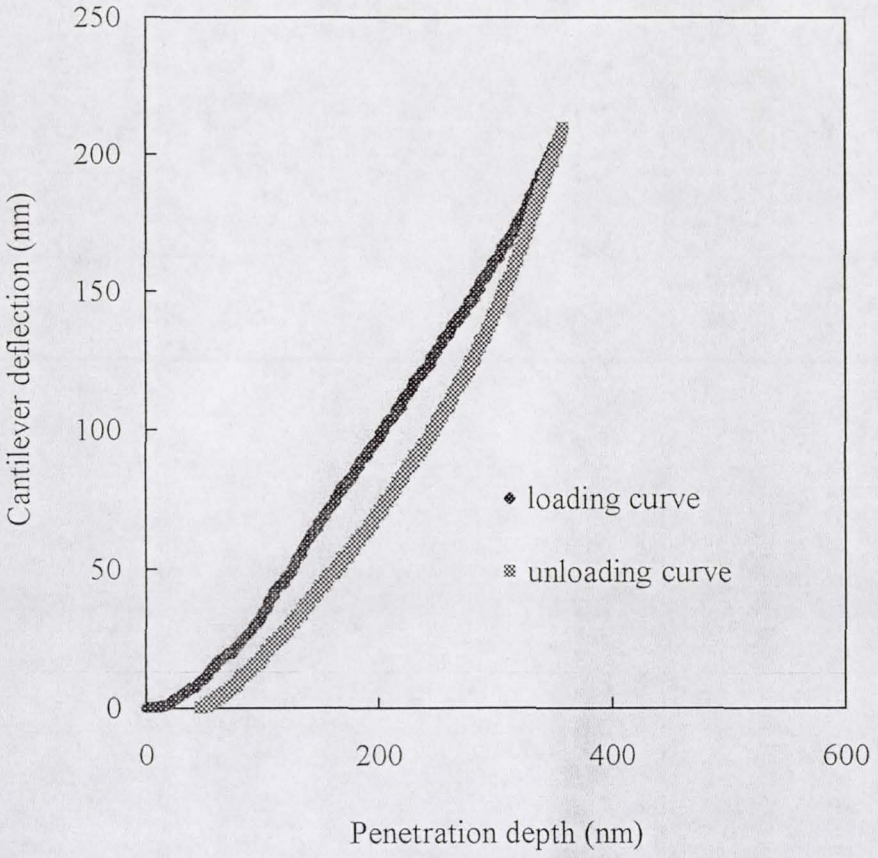

Figure 9 Cantilever deflection (nm) vs. penetration depth (nm) for an un-oxidized PMR-15 polyimide sample using a silicon probe (46#6) with the TopoMetrix TMX 2100

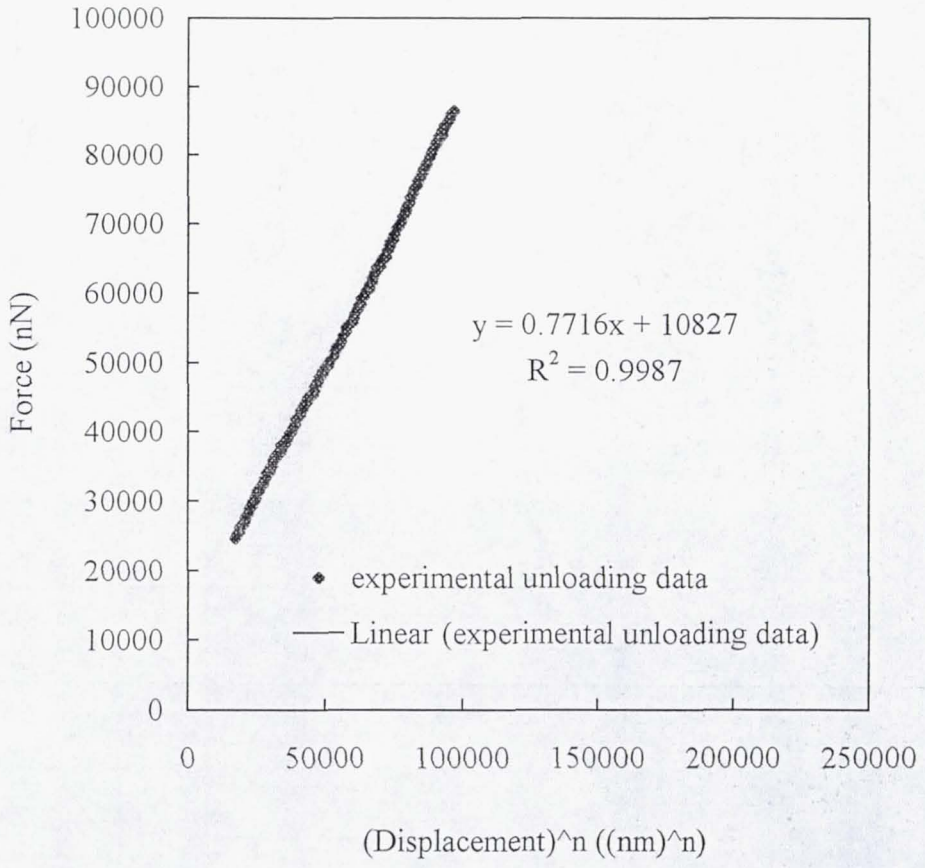

Figure 10 Force (nN) vs. (displacement)^n ((nm)^n) of an un-oxidized PMR-15 polyimide sample using a silicon probe (46#6) with the TopoMetrix TMX 2100

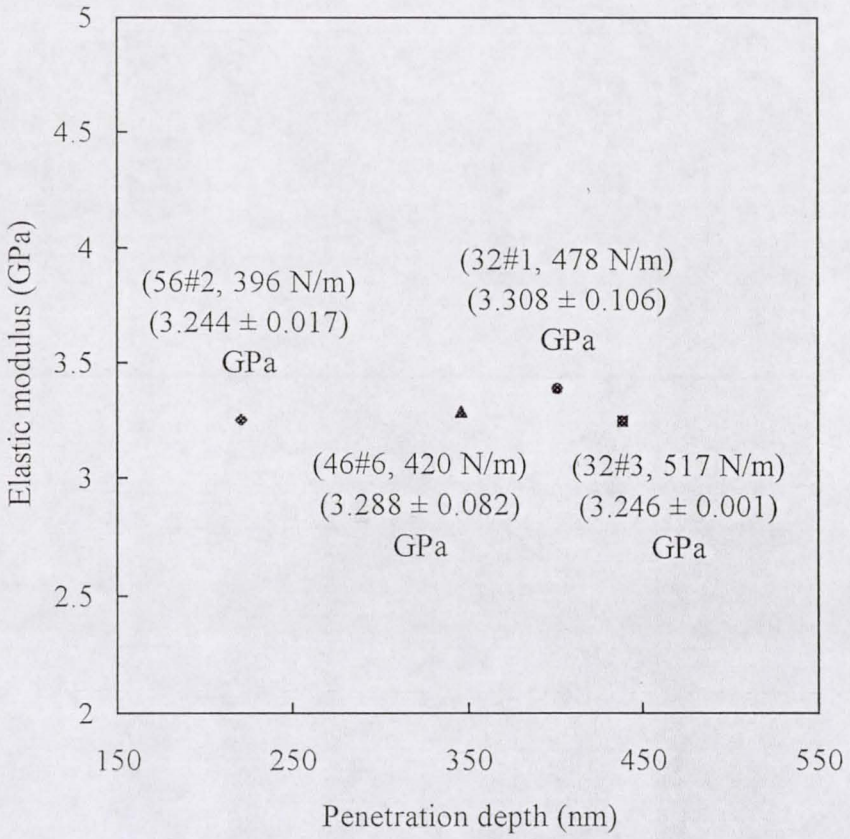

Figure 11 The elastic modulus (GPa) of un-oxidized PMR-15 polyimide samples determined as a function of penetration depth (nm) using four silicon probes with the TopoMetrix TMX 2100

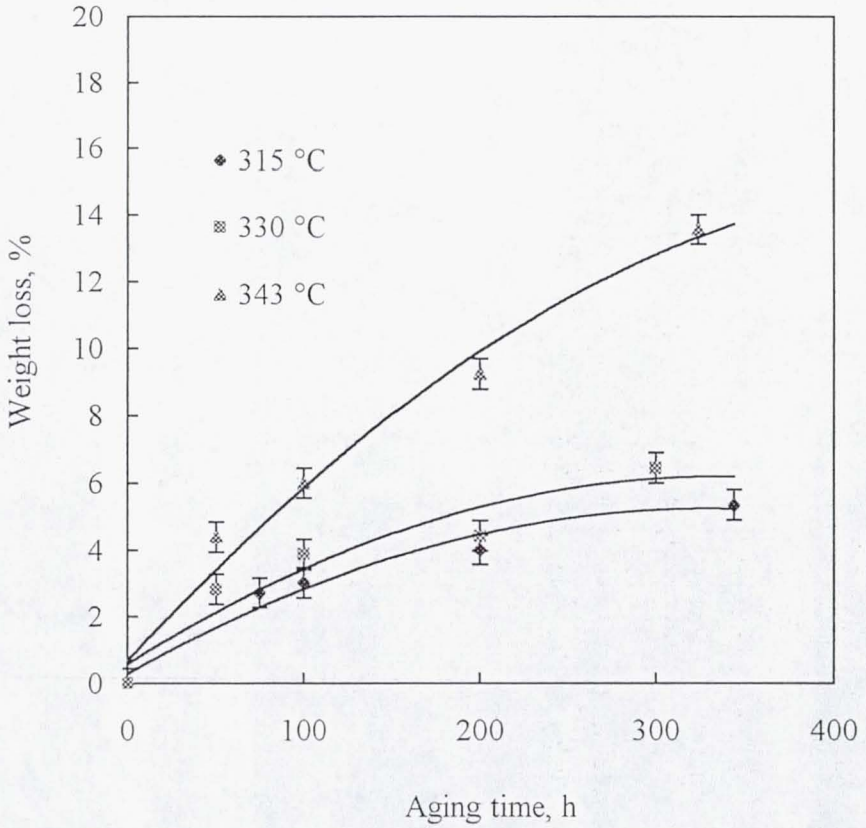

Figure 12 PMR-15 polyimide weight loss in air at different temperatures. The error bar gives the standard deviation.

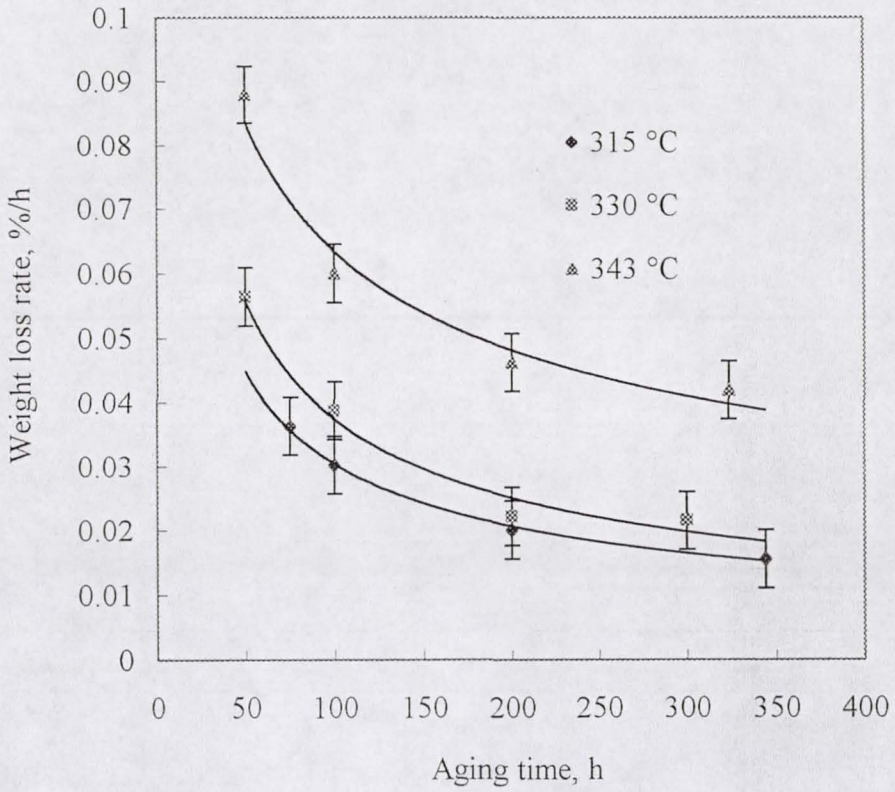

Figure 13 PMR-15 polyimide weight loss rate in air at different temperatures. The error bar gives the standard deviation.

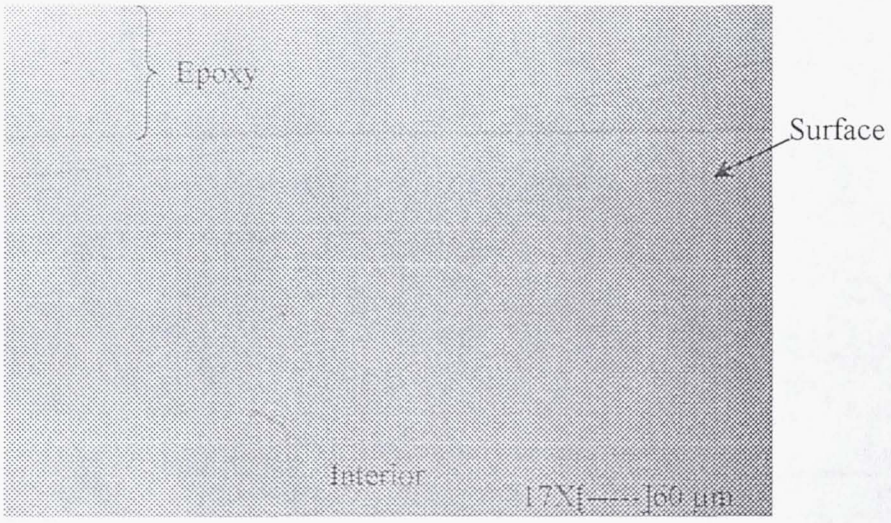

Figure 14 Surface feature of un-oxidized PMR-15 polyimide

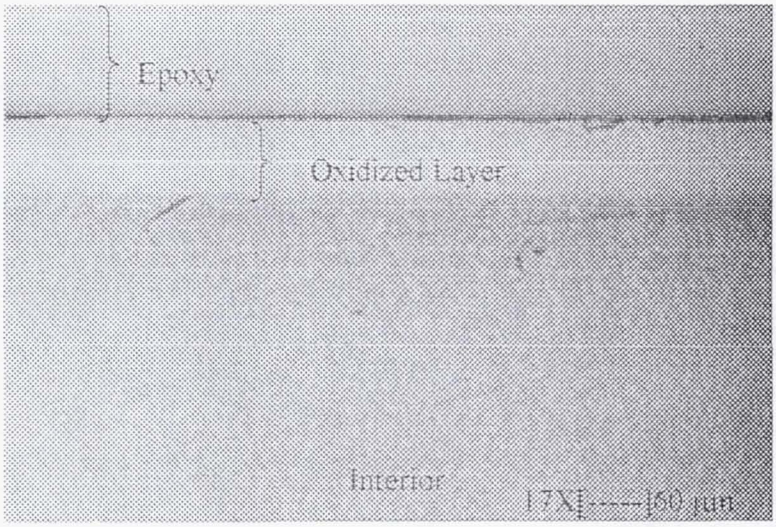

Figure 15 PMR-15 polyimide surface degradation after aging in air at 315 °C for 100 h

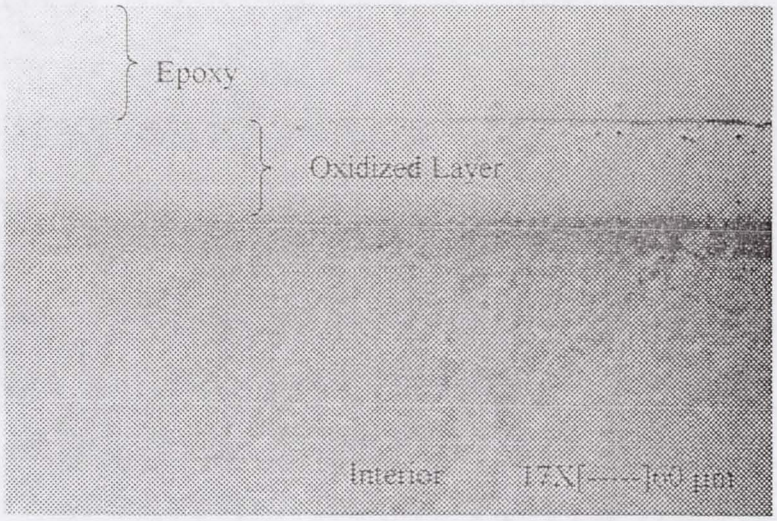

Figure 16 PMR-15 polyimide surface degradation after aging in air at 315 °C for 200 h

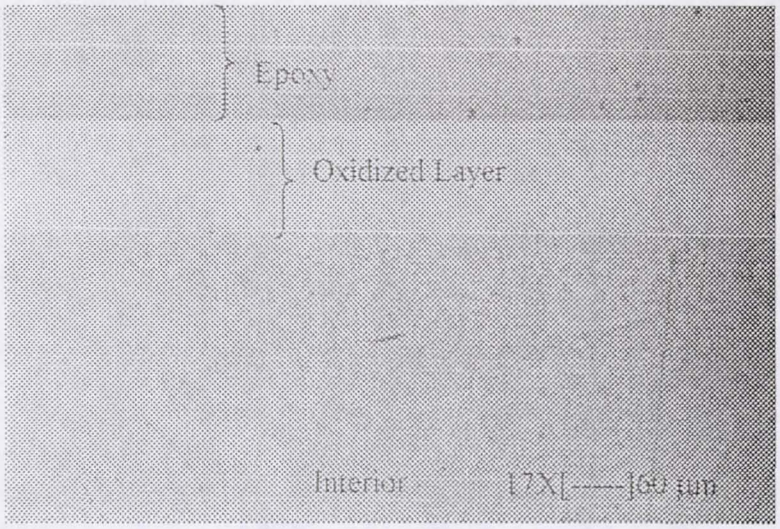

Figure 17 PMR-15 polyimide surface degradation after aging in air at 315 °C for 344 h

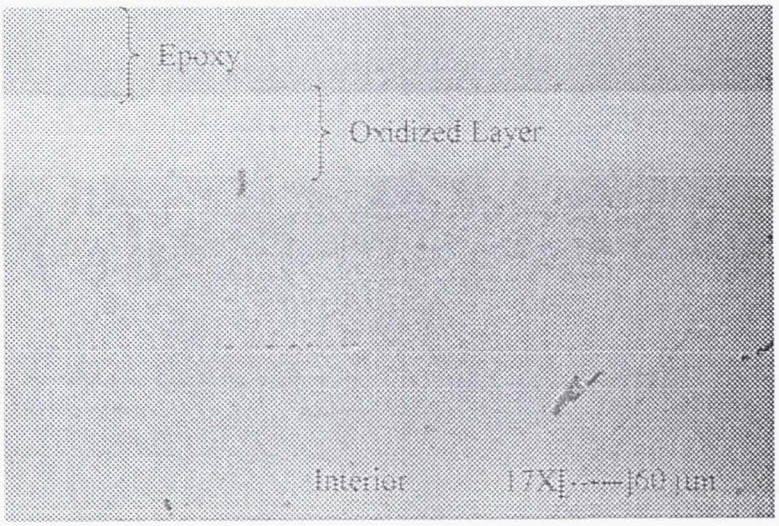

Figure 18 PMR-15 polyimide surface degradation after aging in air at 330 °C for 100 h

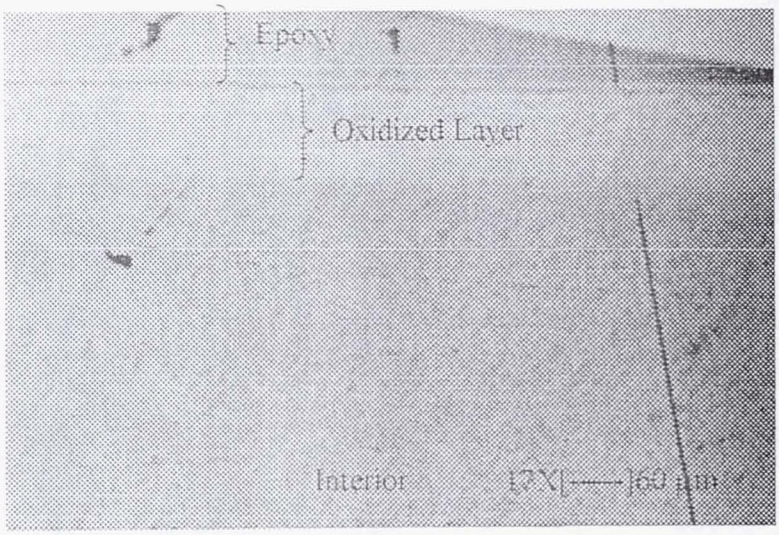

Figure 19 PMR-15 polyimide surface degradation after aging in air at 330 °C for 200 h

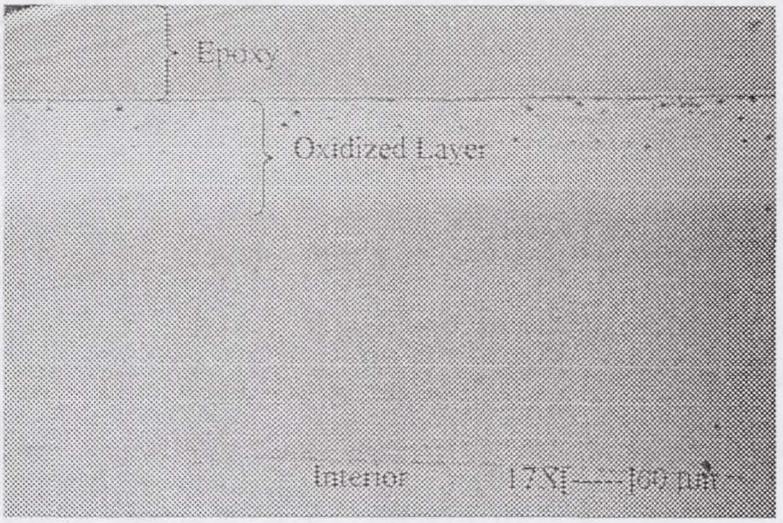

Figure 20 PMR-15 polyimide surface degradation after aging in air at 330 °C for 300 h

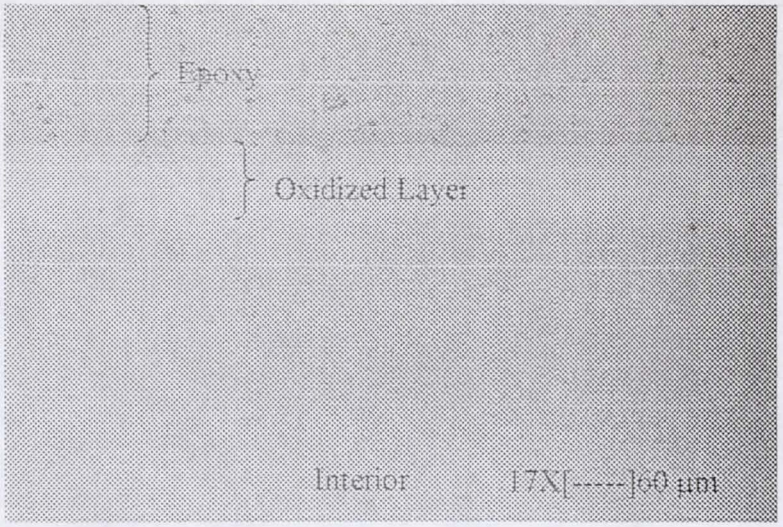

Figure 21 PMR-15 polyimide surface degradation after aging in air at 343 °C for 100 h

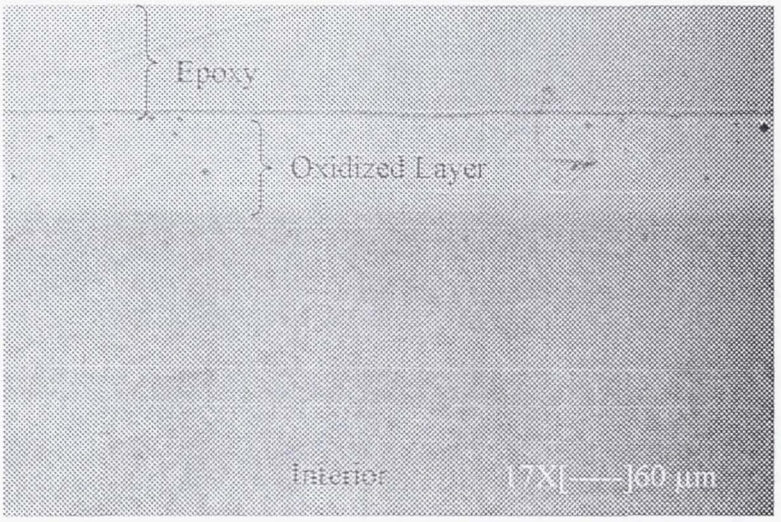

Figure 22 PMR-15 polyimide surface degradation after aging in air at 343 °C for 200 h

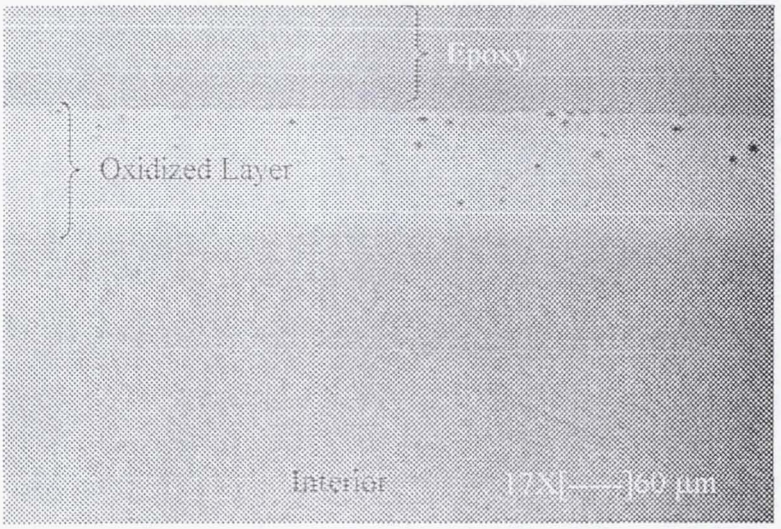

Figure 23 PMR-15 polyimide surface degradation after aging in air at 343 °C for 324 h

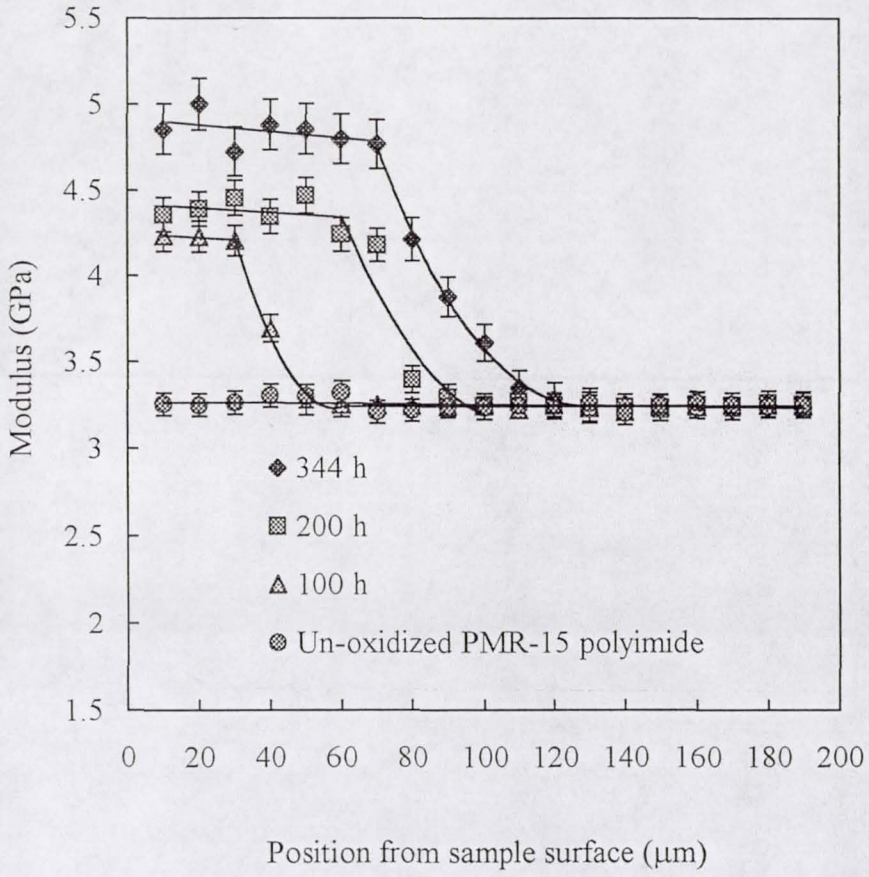

Figure 24 Modulus profiles of PMR-15 polyimide samples aged in air at 315 °C at three different time scales and un-oxidized PMR-15 polyimide sample used as reference. The error bar gives the standard deviation.

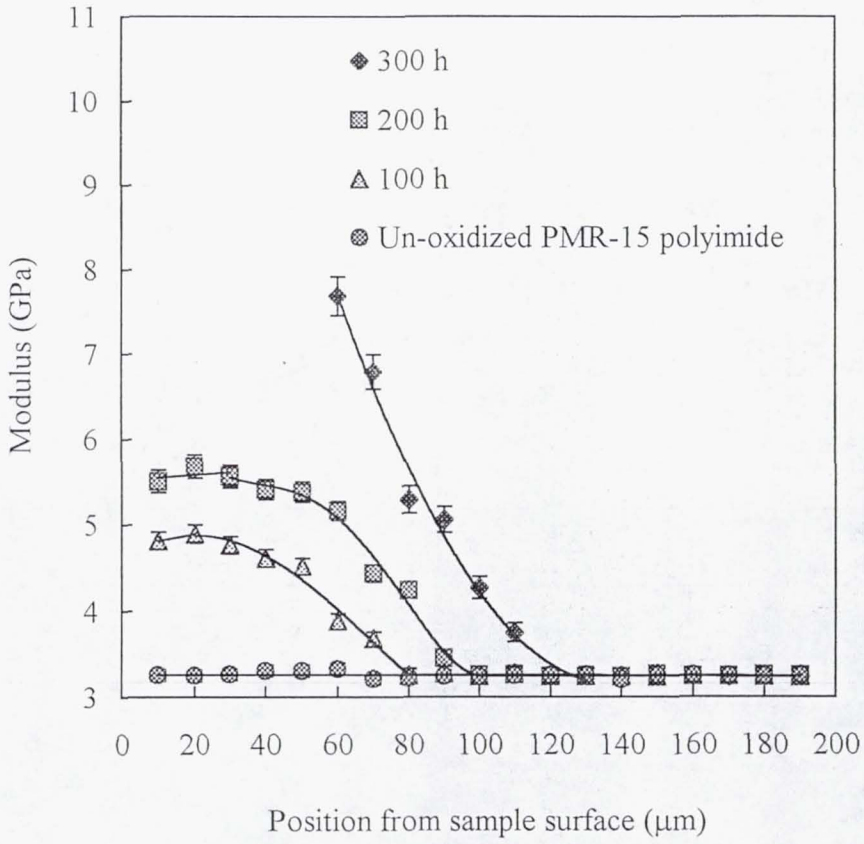

Figure 25 Modulus profiles of PMR-15 polyimide samples aged in air at 330 °C for three different time scales and un-oxidized PMR-15 polyimide sample used as reference. The error bar gives the standard deviation.

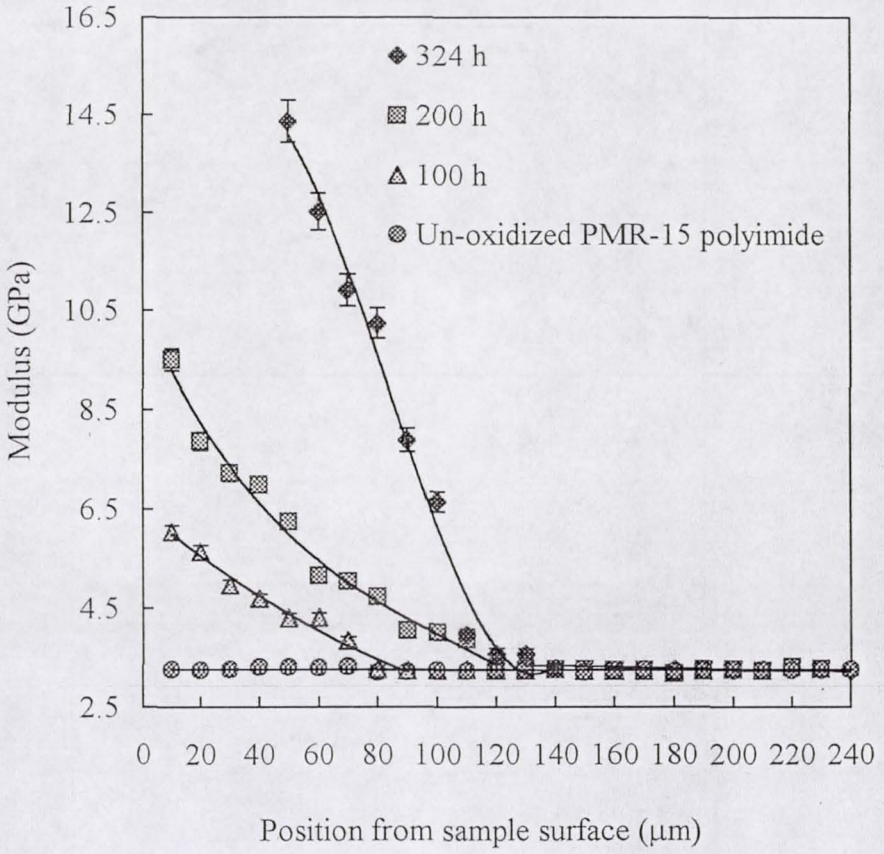

Figure 26 Modulus profiles of PMR-15 polyimide samples aged in air at 343 °C for three different time scales and un-oxidized PMR-15 polyimide sample used as reference. The error bar gives the standard deviation.

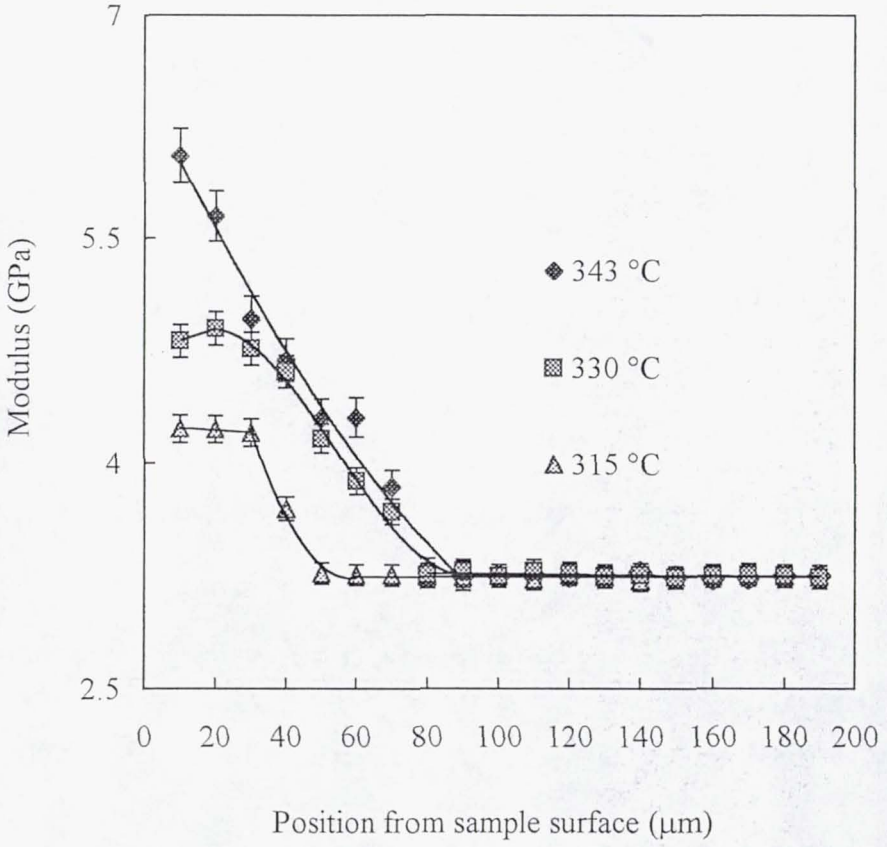

Figure 27 Modulus profiles of PMR-15 polyimide samples aged in air at three different temperatures for 100 h

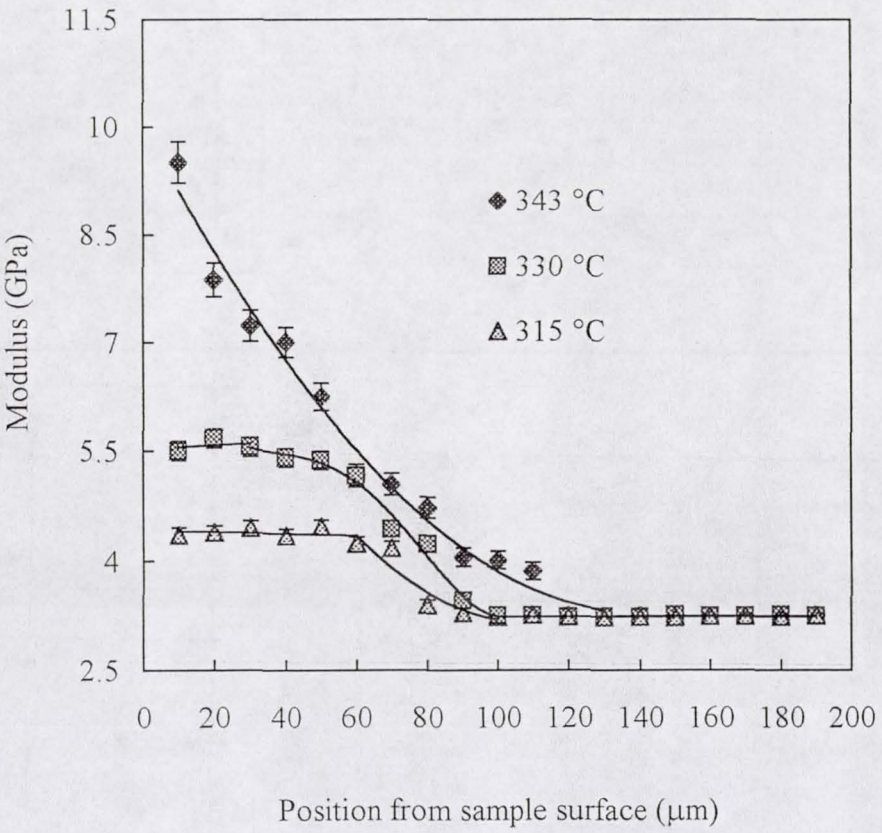

Figure 28 Modulus profiles of PMR-15 polyimide samples aged in air at three different temperatures for 200 h

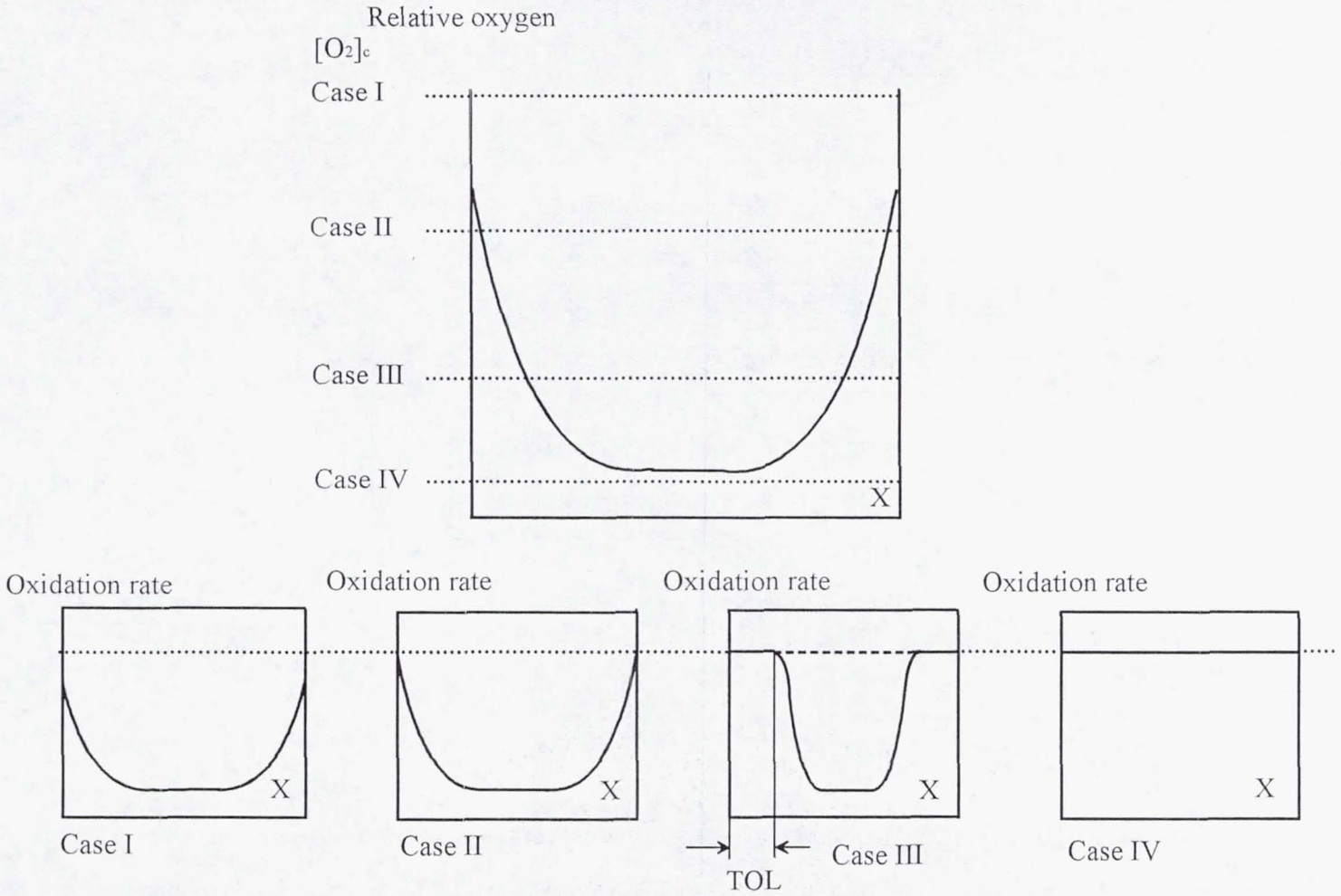

Figure 29 Variation of the shape of the profile as a function of the critical oxygen concentration [27]

Table 1 Geometry parameters and elastic modulus obtained for testing experimental conditions using epoxy, un-oxidized PMR-15 polyimide, and a silicon probe (56#2)

date of experiments (measurements taken at ten different locations)								
January 5th, 2000			January 7th, 2000			January 13th, 2000		
contact geometry (ξ)	tip geometry (n)	elastic modulus (E, GPa)	contact geometry (ξ)	tip geometry (n)	elastic modulus (E, GPa)	contact geometry (ξ)	tip geometry (n)	elastic modulus (E, GPa)
0.184	2.200	3.246	0.186	2.063	3.246	0.194	2.138	3.232
0.221	2.207	3.247	0.179	2.046	3.251	0.193	2.243	3.246
0.206	2.398	3.253	0.180	2.107	3.236	0.183	2.176	3.246
0.179	2.253	3.256	0.178	2.113	3.245	0.182	2.150	3.257
0.201	2.073	3.281	0.178	2.015	3.250	0.191	2.230	3.202
0.179	2.112	3.238	0.179	2.059	3.234	0.193	2.136	3.247
0.188	2.093	3.240	0.174	2.069	3.242	0.175	2.111	3.261
0.188	2.185	3.252	0.184	2.027	3.257	0.186	2.155	3.253
0.182	1.991	3.228	0.181	2.056	3.246	0.187	2.131	3.242
0.178	2.017	3.292	0.179	2.046	3.243	0.175	2.190	3.253
average 0.190	average 2.153	average 3.253	average 0.180	average 2.062	average 3.245	average 0.186	average 2.166	Average 3.244
standard deviation 0.014	standard deviation 0.115	standard deviation 0.018	standard deviation 0.003	standard deviation 0.030	standard deviation 0.006	standard deviation 0.007	standard deviation 0.041	standard deviation 0.017

Table 2 The average values of geometry parameters and elastic modulus obtained for testing the consistency of tip geometry using four silicon probes, epoxy, and un-oxidized PMR-15 polyimide

probe ID	average value of contact geometry using epoxy	average value of tip geometry using epoxy	average value of elastic modulus using PMR-15 polyimide (GPa)	elastic modulus of PMR-15 polyimide from literature[25] and the percentage deviation from experimental result (GPa)
46#6	0.185 ± 0.013	2.002 ± 0.003	3.288 ± 0.082	3.243 (4.624%)
56#2	0.186 ± 0.007	2.166 ± 0.041	3.244 ± 0.017	3.243 (0.237%)
32#1	0.155 ± 0.006	1.935 ± 0.020	3.308 ± 0.106	3.243 (6.693%)
32#3	0.569 ± 0.036	2.003 ± 0.002	3.246 ± 0.001	3.243 (0.248%)